Tectonophysics 698 (2017) 79–90

Contents lists available at ScienceDirect

Tectonophysics

journal homepage: www.elsevier.com/locate/tecto

Finite-frequency P-wave tomography of the Western Canada Sedimentary Basin: Implications for the lithospheric evolution in Western Laurentia

Yunfeng Chen [a,*], Yu Jeffrey Gu [a], Shu-Huei Hung [b]

[a] Department of Physics, University of Alberta, Edmonton, AB, Canada, T6G2E1
[b] Department of Geosciences, National Taiwan University, Taipei, Taiwan

ARTICLE INFO

Article history:
Received 22 August 2016
Received in revised form 14 December 2016
Accepted 7 January 2017
Available online 10 January 2017

Keywords:
Precambrian cratons
Lithospheric evolution
Upper mantle
Laurentia
Western Canada Sedimentary Basin
Finite-frequency tomography

ABSTRACT

The lithosphere beneath the Western Canada Sedimentary Basin has potentially undergone Precambrian subduction and collisional orogenesis, resulting in a complex network of crustal domains. To improve the understanding of its evolutionary history, we combine data from the USArray and three regional networks to invert for P-wave velocities of the upper mantle using finite-frequency tomography. Our model reveals distinct, vertically continuous high (>1%) velocity perturbations at depths above 200 km beneath the Precambrian Buffalo Head Terrane, Hearne craton and Medicine Hat Block, which sharply contrasts with those beneath the Canadian Rockies (<−1%) at comparable depths. The P velocity increases from −0.5% above 70 km depth to 1.5% at 330 km depth beneath southern Alberta, which provides compelling evidence for a deep, structurally complex Hearne craton. In comparison, the lithosphere is substantially thinner beneath the adjacent Buffalo Head Terrane (160 km) and Medicine Hat Block (200 km). These findings are consistent with earlier theories of tectonic assembly in this region, which featured distinct Archean and Proterozoic plate convergences between the Hearne craton and its neighboring domains. The highly variable, bimodally distributed craton thicknesses may also reflect different lithospheric destruction processes beneath the western margin of Laurentia.

1. Introduction

1.1. Overview

Cratons are ancient cores of continents that have survived secular tectonic evolution since the Precambrian (Jordan, 1975; Pollack, 1986; Hoffman, 1988; King, 2005). Their longevity and stability have been largely attributed to the presence of a thick (>300 km), cold and chemically depleted boundary layer (i.e., tectosphere) that resists the convective disruption from the underlying mantle over billions of years (Jordan, 1975, 1979, 1988; Carlson et al., 2005; Sleep, 2005; Griffin et al., 2009). Although the mechanisms for the formation and growth of cratons have been a subject of active debate, existing theories generally favor three possible origins (Lee et al., 2011; Gerya, 2014): hot plume (Boyd, 1989; Griffin et al., 2003; Arndt et al., 2009), slab subduction (Helmstaedt and Schulze, 1989; Hoffman, 1990; Sambridge and Drijkoningen, 1992; Bostock, 1998; Canil, 2004; Pearson and Wittig, 2008; Snyder et al., 2015) and continental collision (Jordan, 1978; Cooper et al., 2006; Gray and Pysklywec, 2010). Since their formation in the Precambrian, the majority of continental cratons have remained relatively stable, although the underlying lithospheric keels may have undergone considerable modifications through episodic growth and destruction associated with major tectonic events (Gao et al., 2002; Carlson et al., 2004; Foley, 2008; Lee et al., 2011).

Laurentia, the cratonic core of North America, has witnessed protracted lithospheric accretion (Hoffman, 1988, 1989; Villeneuve et al., 1993; Foster et al., 2006; Whitmeyer and Karlstrom, 2007; Pearson and Wittig, 2008; Corrigan et al., 2009; Yuan and Romanowicz, 2010; Darbyshire et al., 2013) and reworking (Ross et al., 1991; Davis et al., 2003; Carlson et al., 2004; Mercier et al., 2009; Frederiksen et al., 2013; Bao and Eaton, 2015; Humphreys et al., 2015; Boyce et al., 2016; Liu et al., 2016) during its extensive evolutionary history dating back to >3 billion years ago (Hoffman, 1988; Hammer et al., 2011). The western margin of this ancient continent, where is currently overlain by the Paleozoic strata in the Western Canada Sedimentary Basin (WCSB), has exhibited evidence of rifting, subduction, collisional orogenesis and melting during the Precambrian (Ross et al., 1991; Villeneuve et al., 1993). These tectonic processes and the associated tectonothermal events may have considerable implications for the stabilization and modification of the mantle lithosphere beneath this region (Ross et al., 1991; Ross, 2002).

In this study we take advantage of recently developed regional seismic arrays in Alberta, in conjunction with the USArray Transportable

* Corresponding author.
E-mail address: yunfeng1@ualberta.ca (Y. Chen).

http://dx.doi.org/10.1016/j.tecto.2017.01.006
0040-1951/

Array (TA) deployed to the south of the WCSB, to map the mantle P-wave velocities. Our focuses are the integrity and characteristics of the lithospheric mantle, which enable an updated appraisal of both the existing tectonic framework and the Precambrian evolutionary history of western Laurentia.

1.2. Geological setting

The WCSB consists of the eastern Canadian Cordillera, a strongly deformed thrust and fold belt overlying the western margin of the Precambrian basement, and two major sedimentary basins (i.e., the Williston and Alberta basins; Wright et al., 1994) near the western margin of the ancestral North American craton. The Precambrian basement of the WCSB, presently buried beneath the thick Phanerozoic sedimentary layers, is a network of the Archean continental fragments assembled along the Proterozoic orogenic belts during a relatively short geological period ca. 2.0–1.8 Ga (Ross et al., 1991). These domains are bounded to the east by the Trans-Hudson Orogen (THO), a Himalayan-scale Paleoproterozoic collisional orogenic belt, and to the west by the accreted terranes of the Phanerozoic Cordillera that overthrusted onto the western margin of Laurentia after the Jurassic period (Dickinson, 2004). Our study region consists of the Archean Rae, Hearne, Medicine Hat Block (MHB) and Wyoming provinces, four microcontinents separated by potential structural discontinuities known as the Snowbird Tectonic Zone (STZ), Vulcan Structure (VS) and Great Falls Tectonic Zone (GFTZ), respectively (Fig. 1).

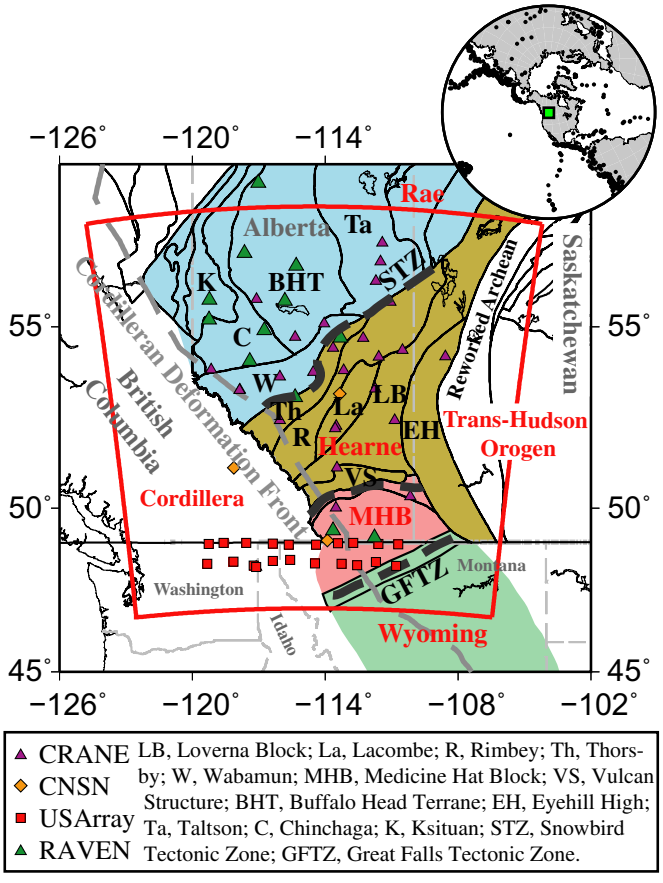

Fig. 1. The tectonic domains in western Laurentia. The red lines mark the boundaries of our velocity model. The black and grey dashed lines indicate the respective locations of major structural discontinuities (i.e., the STZ, VS and GFTZ) and the Cordilleran Deformation Front. The various symbols denote the stations used in this study. The earthquake epicenters are shown in the map inset and the green square marks the region of this study. (For interpretation of the references to colour in this figure legend, the reader is referred to the web version of this article.)

The aforementioned structural discontinuities play a significant role in the interpretation of the regional tectonic history. The STZ can be traced from the exposed portion of the Canadian Shield from northern Saskatchewan to the subsurface in central Alberta, where its delineation is primarily based on potential field anomalies (Ross et al., 1991; Villeneuve et al., 1993). A popular theory attributes its origin to a Proterozoic intercontinental suture (Hoffman, 1988; Berman et al., 2007), resulting from the subduction of an oceanic basin (the Thorsby domain) and the subsequent continent-continent collision between the Archean Rae and Hearne provinces. In this scenario, the Rimbey domain to the southeast of the STZ, which contains 1.79–1.85 Ga old biotite granites, could be associated with a magmatic belt formed during the subduction (Ross et al., 1991; Ross, 2002). Alternative interpretations of the STZ accentuate intracontinental origins such as a shear zone (Hanmer et al., 1995) or an incipient rift (Flowers et al., 2006) based on major metamorphic events (~1.9 Ga) in this area.

The VS in southern Alberta and the GFTZ in northern Montana are equally debated in recent literature. The east-west trending VS is visible from magnetic and gravity observations, separating the Loverna Block (LB), the ancient core of the Hearne craton, from the Archean MHB in the south (Lemieux et al., 2000; Ross, 2002). It was initially proposed to be a rift zone (Kanasewich et al., 1969) but, more recently, a collisional suture according to geophysical analyses (Eaton et al., 1999a; Lemieux et al., 2000). The direction of the dip (north or south; Eaton et al., 1999a; Lemieux et al., 2000) and the age of collision (Archean or Proterozoic; Lemieux et al., 2000; Clowes et al., 2002; Gorman et al., 2002) along the VS remain debated. A similarly controversial structure is the GFTZ, a northeasterly trending potential field anomaly that marks the boundary between the MHB and Wyoming province. While it is more commonly suggested as a convergent margin (Clowes et al., 2002; Gorman et al., 2002; Mueller et al., 2002; Mueller and Frost, 2006), an intracontinental origin cannot be ruled out based on geochemical (Buhlmann et al., 2000) and magnetotelluric observations (Boerner et al., 1998; Meqbel et al., 2014).

1.3. Previous geophysical studies

Potential field data and analyses of U-Pb geochronology of drill core samples of the crystalline basement provided first-order constraints on the configuration of tectonic elements of the WCSB (Ross et al., 1991; Villeneuve et al., 1993). Further refinements to the basement structure were made through multi-disciplinary studies from the Alberta Basement Transects of Lithoprobe (Clowes et al., 1995, 2002; Ross et al., 1995, 2000; Boerner et al., 2000; Ross, 2002), a milestone trans-Canada geophysical experiment. A synopsis of the results from these transects (Eaton et al., 1999a; Lemieux et al., 2000; Ross et al., 2000; Bouzidi et al., 2002) shaped the present-day understanding of the tectonic history of the WCSB, particularly those from the Central Alberta Transect (CAT; Ross et al., 1995, 2000; Eaton and Cassidy, 1996), the Peace River Arch Industry Seismic Experiment (PRAISE) in northern Alberta (Eaton et al., 1999b) and the Southern Alberta Lithospheric Transect (SALT; Eaton et al., 2000; Lemieux et al., 2000; Clowes et al., 2002).

Seismic reflectivity on these transects, in combination with other geophysical observations (e.g., seismic velocity, electrical resistivity and potential fields; Boerner et al., 2000; Hope and Eaton, 2002; Gu and Shen, 2015), played a fundamental role in elucidating the tectonic evolutionary history of central-southern Alberta (Ross, 2002). CAT highlighted the role of the STZ as a collisional boundary (Ross et al., 1995; Eaton and Cassidy, 1996) and revealed thrust-imbricated crust beneath the Hearne province (Ross et al., 1995, 2000). These seismic observations, together with increased mantle conductivity (Boerner et al., 1999; Boerner et al., 2000), led to the "tectonic vise" model in central Alberta (Ross et al., 2000; Ross, 2002), where the Hearne province was suggested to be trapped between oceanic subduction along the STZ in

the northwest (Ross et al., 1991, 1995; Eaton and Cassidy, 1996) and the coeval underthrusting of the THO in the southeast (Lucas et al., 1993; Lewry et al., 1994; Corrigan et al., 2005). The resultant collisional orogen (i.e., east Alberta orogen) was imprinted by substantial *syn*-collisional/*post*-collisional magmatic events, as suggested by the crustal low velocity zones from inversions of receiver functions (*post* Chen et al., 2015) and phase velocities from ambient noise (Gu and Shen, 2015). Additional evidence of pronounced magmatism was provided by the PRAISE transect, which revealed mid-crustal sub-horizontal reflectors (i.e., Winagami reflection sequence) originating from intrusive mafic sheets (Ross and Eaton, 1997; Welford and Clowes, 2006).

In southern Alberta, the Vibroseis Augmented Listen Time (VAULT; Eaton et al., 1999a; Lemieux et al., 2000; Bouzidi et al., 2002) and Deep probe transects of the SALT experiment (Clowes et al., 2002; Gorman et al., 2002) laid the groundwork for a regional tectonic evolutionary model featuring the early Archean amalgamation of the MHB and its subsequent collisions with the Wyoming (south) and Hearne (north) provinces (Clowes et al., 2002; Gorman et al., 2002). This unique assembly process was further supported by a recent magnetotelluric survey in southern Alberta, which attributed the origin of an upper mantle conductor along the VS to an enrichment event during the plate convergence (Nieuwenhuis et al., 2014).

Crustal constraints from Lithoprobe formed the basis of the tectonic framework of the WCSB. Further knowledge of its underlying mantle structures was gained through seismic tomographic imaging, which is sensitive to the thermal, chemical and elastic properties of the upper mantle (Liu and Gu, 2012; Tesoniero et al., 2015). An early effort was made by Shragge et al. (2002) using 11 broadband stations, the model of which revealed high velocities beneath the Archean Hearne province (see Fig. 1 for location) down to ~300 km in central Alberta. Temporal teleseismic experiments in northwestern Canada, e.g., the Canadian Northwest Experiment (CANOE) and the Portable Observatories of Lithospheric Analysis and Research Investigating Seismicity (POLARIS) arrays, enabled more detailed examinations of the crust and upper mantle beneath the Cordilleran portion of the WCSB. Mercier et al. (2009) utilized the data from these networks to invert for the first regional-scale velocity model of the upper mantle in western Canada. The high-resolution images showed a sharp transition in P- and S-wave velocities at the Cordilleran Deformation Front (CDF) from slow Phanerozoic Cordillera to fast Precambrian cratons. This structural transition was further supported by the results of ambient noise tomography at crustal depths (Dalton et al., 2011; Kao et al., 2013). More recently, a surface wave analysis (Bao and Eaton, 2015) that incorporated more broadband sensors in the southern WCSB offered improved seismic constraints on the basement structures. The results of this study provided evidence for deep lithospheric keels beneath the Hearne province and Buffalo Head Terrane (BHT).

Despite the seminal contributions from these earlier broadband analyses, relatively restrictive station distributions and short deployment time presented major challenges to the investigation of the detailed mantle structure beneath the southern WCSB (e.g., central-southern Alberta). These data related issues have been largely resolved by the establishment of regional seismic networks in recent years, most notably the Canadian Rockies and Alberta Network (CRANE; Gu et al., 2011), which initiated in mid-2006, and the Regional Alberta Observatory for Earthquake Studies Network (RAVEN; Schultz and Stern, 2015a). These arrays form the backbone for regional structural analysis (Gu et al., 2011, 2015; Gu and Shen, 2015) and seismicity monitoring (Schultz et al., 2014, 2015b; Wang et al., 2016). By combining all the available recordings from CRANE and surrounding networks, the data volume and distribution far exceed those from earlier broadband seismic analyses in this region. To improve imaging resolution and accuracy further, we adopt the finite-frequency theory (Dahlen et al., 2000; Hung et al., 2000) and high-frequency body wave in the analysis of the spatial correlation between crustal domains and their underlying mantle seismic velocities.

2. Data and method

2.1. Data

This study aims to resolve the details of the mantle lithosphere beneath the WCSB using the most complete broadband seismic dataset to date. Our dataset consists of recordings from 27 stations from the Canadian Rockies and Alberta Network (CRANE), 3 stations from the Canadian National Seismograph Network (CNSN), 12 stations from the Regional Alberta Observatory for Earthquake Studies Network (RAVEN) and 21 stations from the USArray (see Fig. 1). Teleseismic (30–90°) P-wave data from 1566 Mw > 5.5 earthquakes, recorded between 2006 and 2015, are included in this study (see Fig. 1). After removing the instrument responses, vertical component seismograms are filtered (using a fourth-order Butterworth function) into low and high frequency bands with respective ranges of 0.03–0.125 and 0.3–2.0 Hz; these frequency ranges are selected to minimize the effect of a strong noise peak at ~0.2 Hz. We then measure the relative P-wave arrival times for each station pair using the multi-channel cross-correlation method (VanDecar and Crosson, 1990). For all recording stations, the travel-time differences for a specific event are first determined as time delays that lead to the maximum cross-correlation coefficients. Subsequently, these delays are subjected to least-squares optimization, and the final travel-time residuals are calculated by subtracting the demeaned theoretical relative arrival times (AK135; Kennett et al., 1995) from the optimized values. The total numbers of P-wave measurements at low and high frequencies are 11,602 and 9439, respectively.

2.2. Model parameterization and inversion

The travel times are inverted with finite-frequency tomography (Hung et al., 2000, 2004), which is more accurate than ray-based approaches since it considers wave-front healing of frequency-dependent seismic waves (Hung et al., 2000; Montelli et al., 2004; Zhou et al., 2005). Our model parameterizes the study region, which covers most of Alberta and southeastern British Columbia, using a grid of nodes with respective sizes of 40 km, 40 km and 25 km in longitude, latitude and depth. The total number of nodes ($33 \times 33 \times 33 = 35{,}937$) exceeds the number of travel-time measurements (21,041), which poses an ill-conditioned linear system. Thus we adopt an adaptive, wavelet-based multi-scale parameterization to minimize the effect of uneven data sampling (Chiao and Kuo, 2001; Hung et al., 2010; see Fig. 1) and solve for perturbations in P-wave velocities using the LSQR algorithm (Paige and Saunders, 1982). Event and station correction terms are also included in the matrix to properly account for source-side structures and the travel-time fluctuations associated with shallow crustal anomalies beneath the receivers (Hung et al., 2004). The optimal model solution is determined by choosing the damping parameter associated with the turning point on the trade-off curve between model norm and variance reduction. More details on the finite-frequency theory and multi-scale parameterization can be found in Hung et al. (2011).

3. Result

3.1. Resolution test

The use of finite-frequency kernel leads to higher resolution in the recovered mantle seismic structure. To illustrate this we compute the "hit-count" maps, which indicate the overall sensitivities of P-wave travel-time data contributing to the spatial grid nodes used in this study (Fig. 2). In comparison with ray-based approaches, which are mainly sensitive to localized zones around the receivers (see right panel in Fig. 2), the overall resolution provided by finite-frequency kernel is more uniform across the study region (see left panel in Fig. 2), especially at shallow (e.g., 100 km) depths.

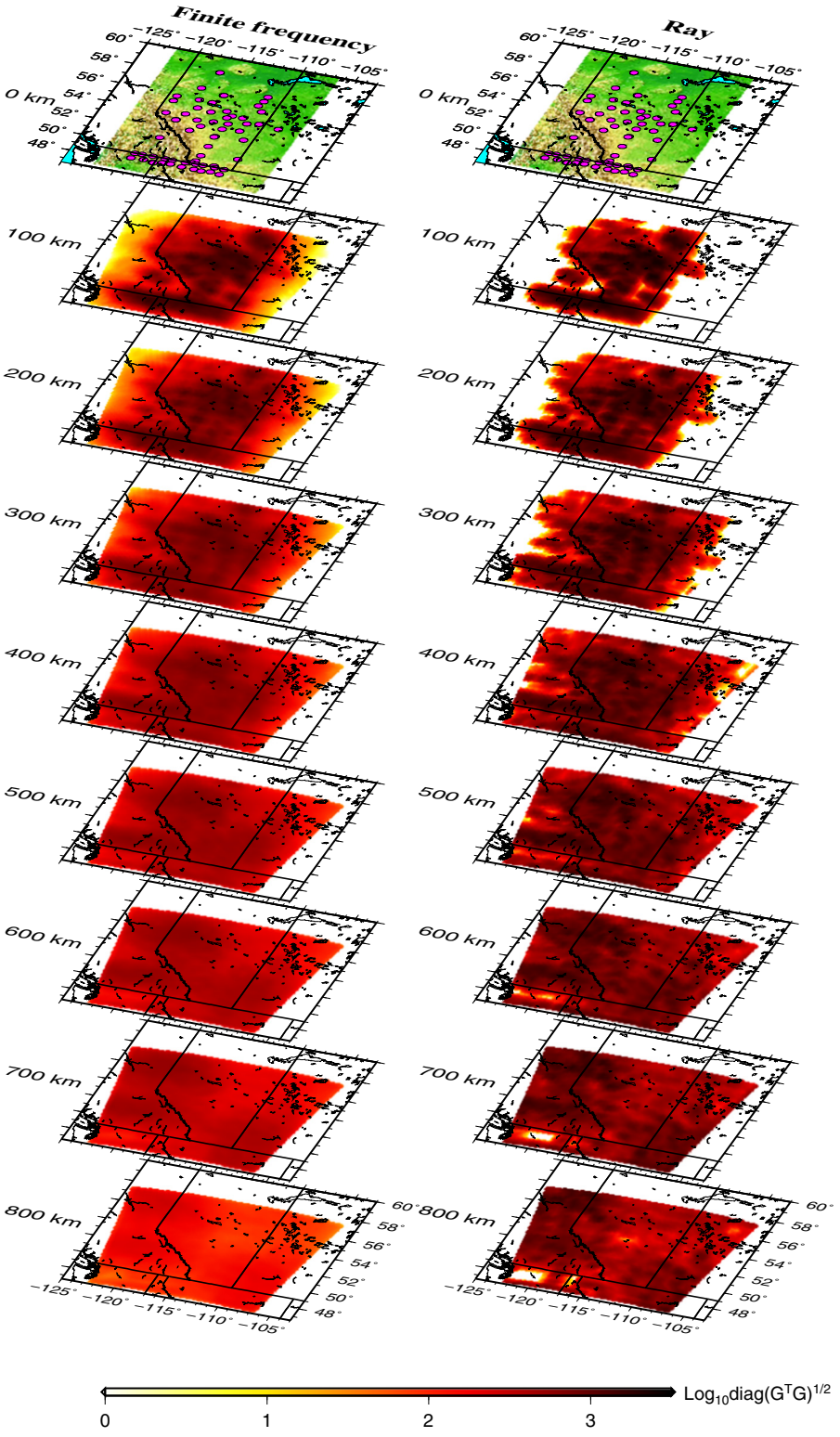

Fig. 2. "Hit-count" maps showing the diagonal elements of the resolution matrix (diag(G^TG)) at various mantle depths, which reflect the data coverage and overall sensitivity of the inversion kernel. The finite-frequency results show improved nominal resolution in central Alberta, especially at shallow mantle depths, due to the use of the Fresnel volumes of the seismic waves.

To quantify the robustness of the travel-time inversion, we perform a "checkerboard" resolution test by constructing a hypothetical input structure with $\pm 2.5\%$ alternating Gaussian-shaped anomalies relative to the background velocity (Fig. 3). Each anomaly is represented by 6 nodes in all three directions, which result in a volume of $230 \times 230 \times 150$ km^3. Synthetic travel times are calculated based on realistic event-station geometries, and random noise up to 50 msec (comparable to the noise level of the data) is subsequently added. The recovered models (Fig. 3b–d) show nearly 80% recovery of the maximum amplitude. The lateral resolution is superior in central-southern

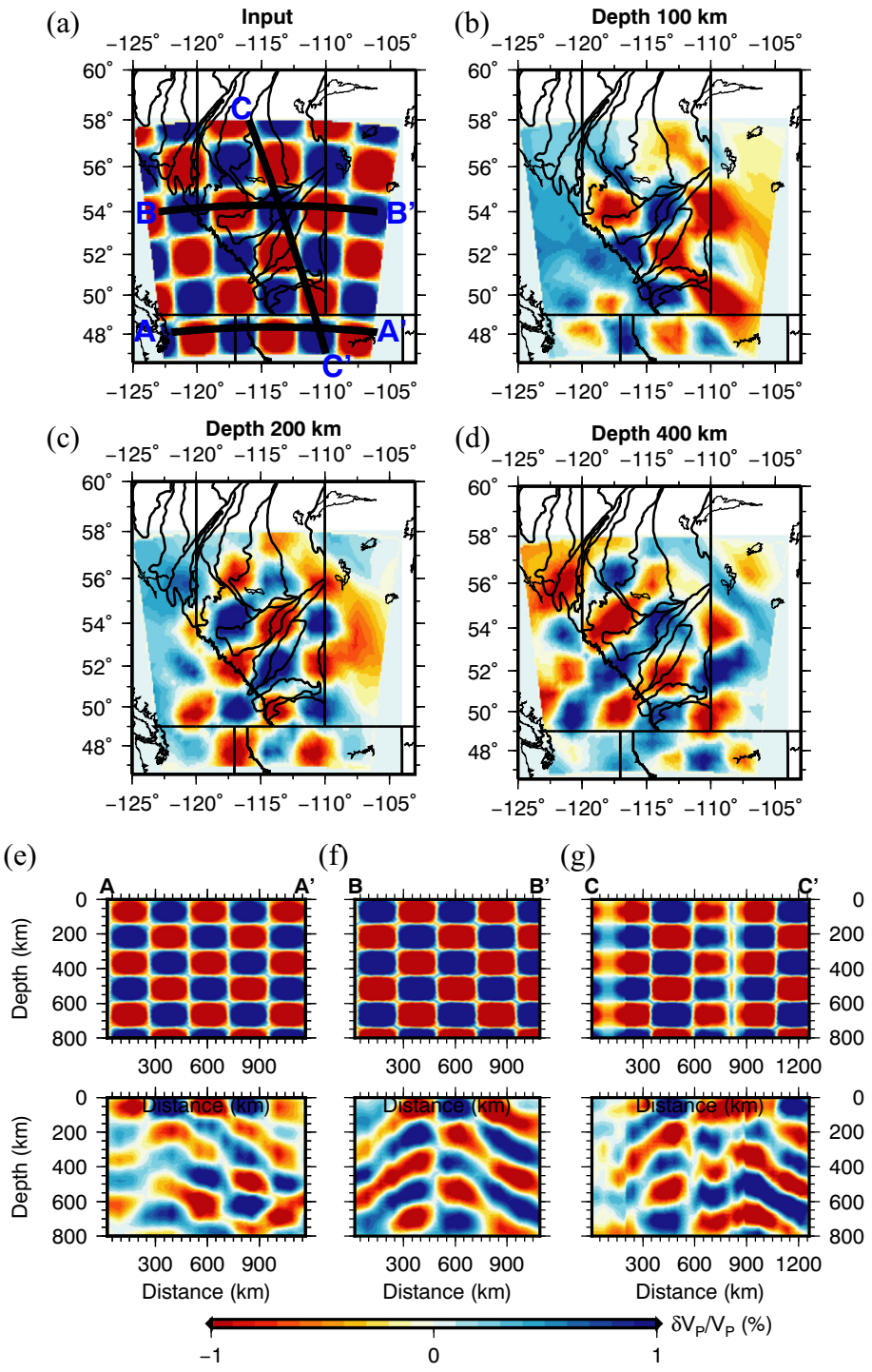

Fig. 3. "Checkerboard" test using 2.5% alternating positive and negative Gaussian-shaped anomalies. (a) Input structure at 100 km depth. (b)–(d) Output velocity models at 100, 200 and 400 km depths, respectively. (e)–(g) Input (top panels) and output (bottom panels) structures for three cross-sections shown in (a).

Alberta where relatively dense station coverage is available (see Fig. 1 for station locations). The recovered velocity anomalies north of 55° N become weaker and more diffuse due to a relatively sparse distribution of stations. The vertical resolution (Fig. 3e–g) is sufficient to differentiate between the alternating velocity anomalies, despite minor lateral and oblique smearing effects. The maximum vertical resolution is observed in the depth range of 100–400 km, where a large number of crossing ray paths are available; this is ideal for imaging the depth and characteristics of the lithosphere.

3.2. General assessment of the upper mantle

The P-wave model from our finite-frequency travel-time tomography shows two groups of prominent seismic anomalies at the depths above 300 km in the upper mantle: 1) a low velocity zone beneath the Rockies, and 2) a broad high velocity region under the Precambrian basement of Alberta (Fig. 4a). The P velocity increases by >2% from the southern Canadian Cordillera (<−1%) to the Alberta basin (>1%) within a lateral distance of 50 km (Fig. 4b). This sharp (>2%) eastward

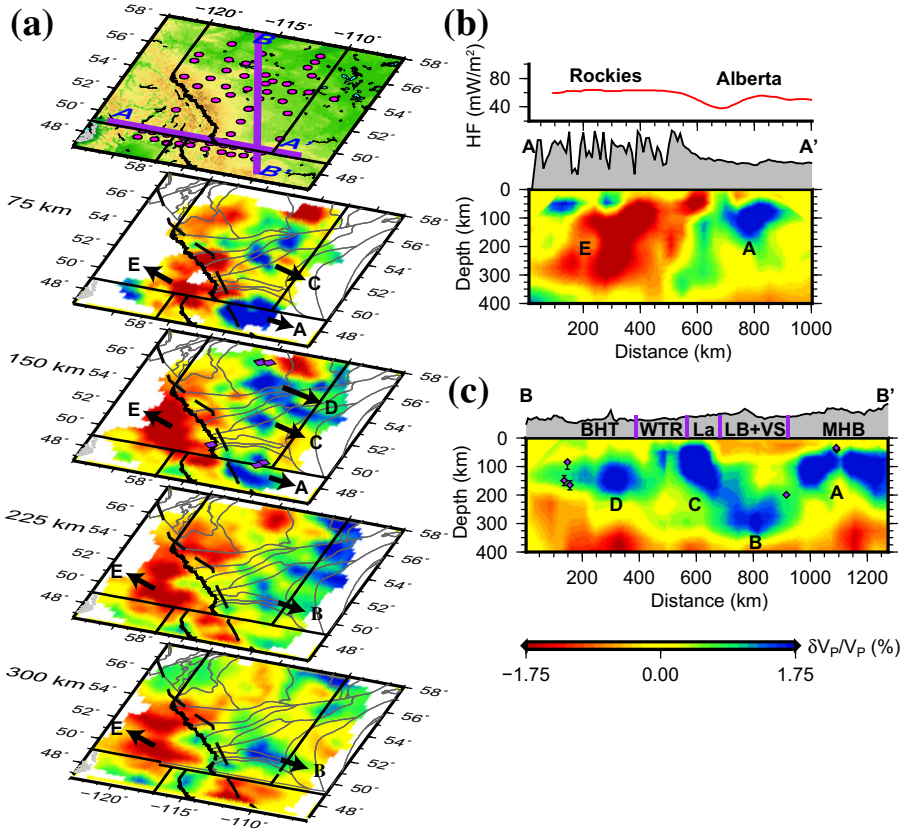

Fig. 4. (a) P-wave velocities at four mantle depths. Poorly sampled grids have been removed prior to plotting. The purple lines and circles superimposed on surface topography indicate the locations of the profiles and stations, respectively. Five major anomalies have been labeled. The tectonic domain boundaries and the Cordilleran Deformation Front are indicated by the thin solid and thick dashed lines, respectively. The locations of mantle xenoliths (Buhlmann et al., 2000; Canil et al., 2003; Aulbach et al., 2004) are plotted at 150 km depth. (b) P velocity perturbations along the AA' profile. The topography is shaded in grey and heat flow (Majorowicz, 2016) is plotted above the surface topography. (c) Similar to (b), but for profile BB'. The purple lines mark the locations of the domain boundaries and the diamond symbols indicate the reported locations of xenoliths projected onto the cross-section. The error bars indicate the depth range of xenoliths. WTR: Wabamun, Thorsby and Rimbey. See Fig. 1 caption for the other abbreviated domain names. (For interpretation of the references to colour in this figure legend, the reader is referred to the web version of this article.)

increase in seismic velocity coincides with the steep (1000 m) topographic relief and a reduction in heat flow by 20 mW/m^2 (see Fig. 4b), which imply different thermal regimes in the upper mantle between the Cordillera and the adjacent craton(s) (Frederiksen et al., 2001; Lewis et al., 2003; Mercier et al., 2009; Hyndman, 2010; Hyndman and Currie, 2011; Kao et al., 2013).

The distribution of high velocities east of the Cordillera, the main focus of this study, shows significant spatial variations among the known basement domains of the WCSB (Ross et al., 1991; Villeneuve et al., 1993). In the depth range of 75–150 km, we identify distinct zones of high (>2%) velocities (see Fig. 4a) beneath the Precambrian provinces Hearne (C), BHT (D) and MHB (A). The latter two anomalies (A and D) become less significant (<0.5%) at ~200 km (see map at 225 km depth in Fig. 4a), below which the P velocities quickly become indistinguishable from the surrounding mantle (e.g., at 300 km depth). On the other hand, the high velocity zone beneath the Hearne province (anomaly C) exhibits downward continuity, extending obliquely to 350 km depth or greater (see B in Fig. 4a). This deep, circular-shaped anomaly (with a rough radius of 200 km) is characterized by ~1.5% positive velocity perturbations, spanning the entire area within the crustal domain boundaries of the LB. The P velocity decreases to −0.5% at depths above ~70 km, which is representative of a low velocity structure at crustal-shallow mantle depths.

3.3. Hypothesis test

The presence of relatively small-scale anomalies (e.g., the low velocities down to 75 km at location B, see Fig. 4c) inevitably raises questions about the sensitivity of our dataset to secondary heterogeneities. To further assess the resolving power of the data, we perform three groups of hypothesis tests with input models (top panels in Fig. 5) that capture the geometries of the main findings detailed in Section 3.2 (see Fig. 4c). The amplitudes of the input low and high velocity anomalies are −2% and 1.5–3%, respectively, to account for the effects of damping and smoothing in the inversion. All synthetic tests adopt the same data coverage and choice of damping as those used in the actual inversion. The first group of models contain a 1.5% low velocity layer with variable thicknesses ranging from 25 to 75 km, which correspond to layers 1–3 of the parameterized model (Fig. 5a–c). Our inversion can recover 60% of the maximum amplitude of the input low velocity structures with thicknesses >50 km, but a 25 km thick layer is beyond the resolution of the data. Both the lateral and vertical dimensions of the input structures are reasonably constrained with minimal smearing effects. In the second test group, we introduce a 1.5% positive anomaly in the shallow mantle (Fig. 5d–f). The model recovery is comparable to those of the first group, except that the boundary between the crust and upper mantle is less apparent after the inversion. This suggests limited vertical resolution to sharp changes within the crust and the top 20–30 km of the upper mantle. In the final series of tests (Fig. 5g–i), we reduce the lateral dimension of the low velocity layer to half its original size, which approximately equals to the width of the VS inferred from the domain boundaries. With a recovery of 50% of the input amplitude, the outcome is satisfactory for an input 50–75 km thick low velocity layer despite a slightly reduced lateral dimension.

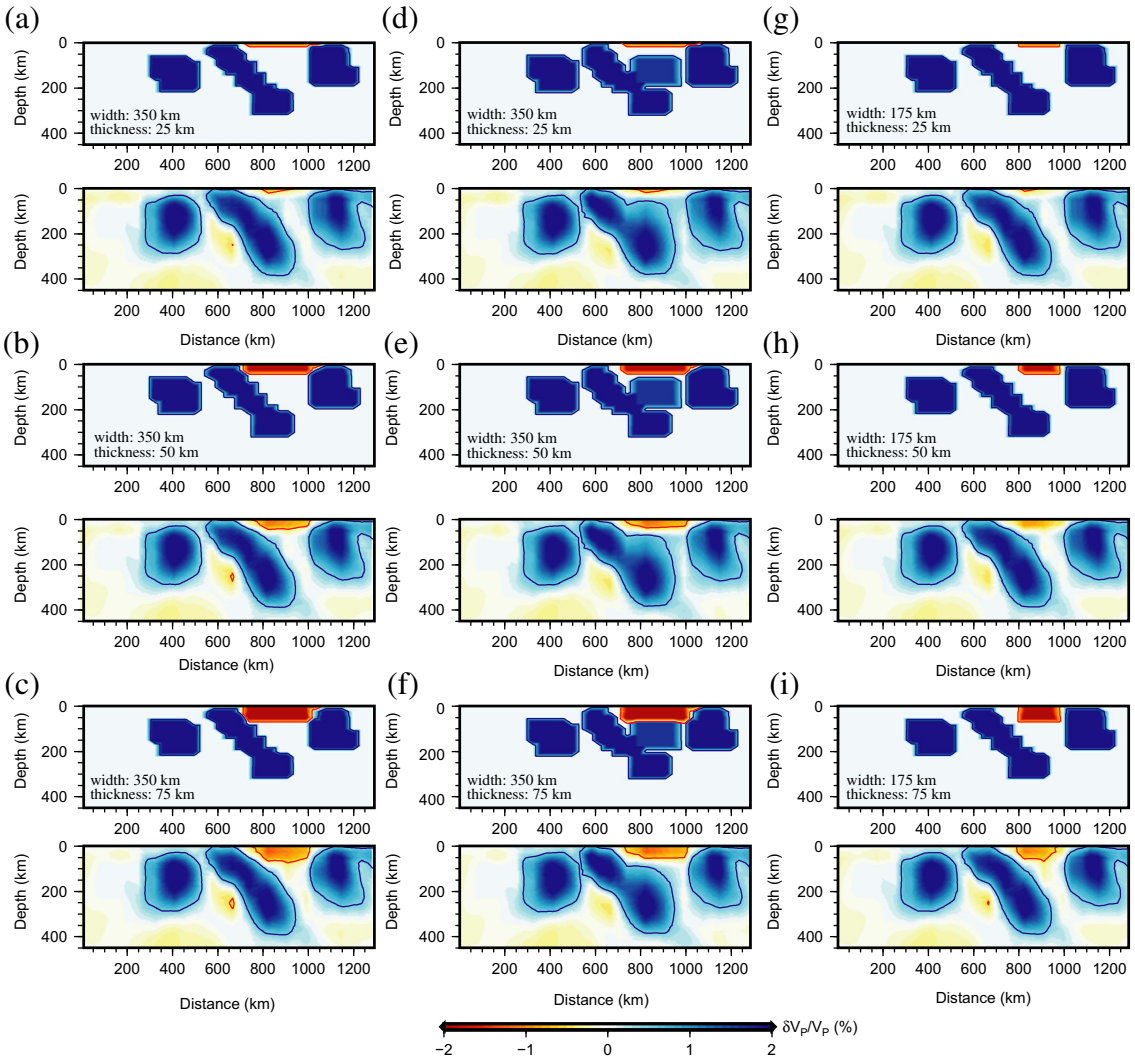

Fig. 5. Hypothesis tests with variable input upper mantle structures (top panels). The output models (bottom panels) are recovered using the same data coverage and smoothing parameters as those from the actual inversion. The widths and thicknesses of the input low velocity anomalies are labeled.

3.4. Depth extent of cratons

The dense regional teleseismic data enable us to examine the vertical extent of cratonic structures in western Laurentia at a higher resolution than before. We associate the high velocity anomalies to the east of the CDF with the mantle lithosphere beneath Precambrian cratons, which assumes vertically continuous structures from crust to mantle (i.e., crustal and mantle age are correlated; Lee et al., 2011) due to the lack of reported mantle age from geochronological dating in the study region. To determine the depths of the cratons we compute the average 1D velocities corresponding to the high velocity zones labeled in Fig. 4 (Fig. 6a). The P velocities are vertically continuous below the MHB (A), Lacombe domain (C) and BHT (D) down to ~200 km depth, with positive perturbations in excess of 1% (Fig. 6b); these are nearly opposite to the velocities (<−1%) beneath the Rockies (E). The mantle beneath the southern Hearne province (B) is visibly more complex, showing a velocity reversal from low (−0.5%) to high (0.5%) values at ~180 km depth (see the shaded area in Fig. 6b). To determine the base of the lithosphere at a given region, we compute the velocity derivatives with respect to depth. Assuming the base of the craton is defined by the depth of the maximum negative velocity gradient (Priestley and Debayle, 2003; Hopper and Fischer, 2015), the depths of the lithosphere beneath the MHB (A), southern Hearne province (B), Lacombe domain (C) and BHT (D) are 230 km, 350 km, 220 km and 185 km, respectively. These values are determined based on the assumptions that 1) the background velocity model (e.g., AK135 model) contains a relatively constant velocity gradient at lithospheric depths and 2) the P-wave velocity transition is generally sharp across the lithosphere-asthenosphere boundary (LAB). The former criterion results in uncertainties that are <10 km (see Supporting information Text S3), which are considerably smaller than the vertical resolution of body waves. The latter assumption is favored by strong S-to-P converted phases resulting from the depth of a potential LAB (Fischer et al., 2010).

Because the depth extents of the seismic anomalies are often overestimated by body-wave tomography due to the effect of vertical smearing, it is critical to assess the degree of overestimation in our model space and make the appropriate corrections. To do so, we calculate the difference of the craton depths between the input (150–325 km) and output average 1D velocity models based on the hypothesis test (see models in Fig. 5e). In this synthetic example, the base of the lithosphere is determined using the same criterion (i.e., the maximum negative velocity gradient) as that of the actual observation. The resultant raw craton depths from the recovered models overestimate those of the ground truth (i.e., input values) by 16 to 38 km, depending on the region (Fig. 6c).

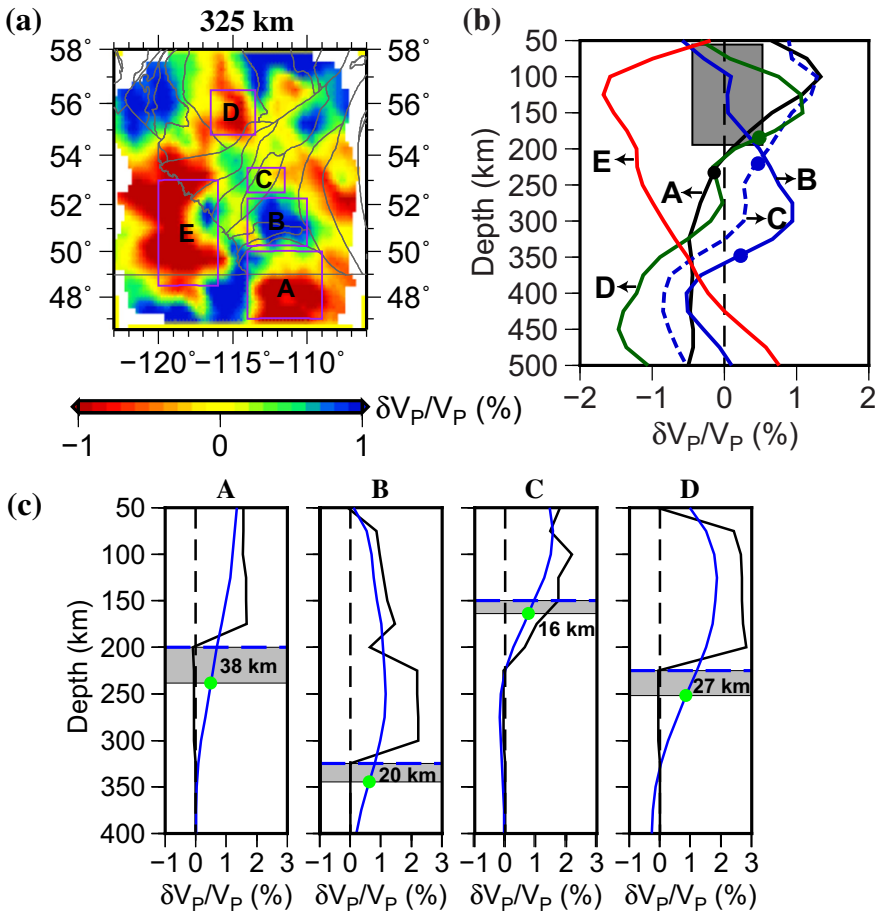

Fig. 6. (a) P-wave velocity perturbations at 325 km depth. The enclosed regions highlight the lateral extents of major upper mantle anomalies. (b) Average 1D velocities computed from the regions defined in (a). The circles mark the base of the cratons. The shaded area highlights a low velocity mantle in region B. (c) Average 1D velocities of four cratonic regions calculated from the hypothetical input (black) and output (blue) models shown in Fig. 5e. The craton depths of the input and output models are marked by the blue dashed lines and green circles, respectively. The shaded areas indicate variable amounts of vertical smearing. The base of the Lacombe domain (region C) is not well defined due to the dipping input structure (see Fig. 5). (For interpretation of the references to colour in this figure legend, the reader is referred to the web version of this article.)

3.5. Comparison of craton depths

After correcting for the vertical smearing (~20 km, see Fig. 6c and Section 3.4), we obtain a cratonic root of ~330 km beneath the southern Hearne province (region B). This observation is consistent with an earlier finding (~300 km) from body wave tomography (Shragge et al., 2002), though it is considerably deeper than a recent estimate (~260 km) from surface waves (Bao and Eaton, 2015). Garnet xenocrysts from the southwestern margin of the Hearne province (see Fig. 4a for the kimberlite location) suggest a mantle root that was at least 200 km deep in the Triassic (Canil et al., 2003). This value is considerably shallower than our estimate (330 km), though the preferential distribution of kimberlites around the craton margins, instead of at the centers (Griffin et al., 2009), may be partially responsible. A recent magnetotelluric survey reported a 250 km deep craton beneath the MHB and southern Hearne (Nieuwenhuis et al., 2014), which falls well within our respective estimates of 200 km and 330 km.

Further north, our estimated craton thickness decreases to ~200 km beneath the Lacombe domain, a subdivision of the Hearne province consisting of low-grade metavolcanic and metasedimentary rocks with age <2.3 Ga (Ross et al., 1991). Beneath the BHT, a Proterozoic (1.99–2.34 Ga) component of the predominantly Archean Rae province (Ross, 2002), the thickness of the lithosphere becomes ~185 km (160 km after correction), which is over 100 km thinner than that beneath the Hearne province. This value is generally consistent with the LAB depth estimates from xenoliths (180 km; Aulbach et al., 2004; see Fig. 4a for sample locations), electrical resistivity (180–220 km; Türkoglu et al., 2009) and heat flow (200 km; Majorowicz et al., 2014) data, but it is significantly shallower than the reported value (260 km; Bao and Eaton, 2015) from surface wave tomography.

4. Discussion

4.1. Global comparison of craton depths

Lithospheric thicknesses in western Laurentia enable a systematic comparison with those of other cratons. On a global scale, the reported depths of the cratonic roots from tomographic models can vary by 100 km or more (Fig. 7a). Assuming coeval continental crust and mantle formation (Lee et al., 2011), the relatively intact cratons examined in recent literature exhibit no significant correlation between crustal age and lithospheric thickness (Simons and Van Der Hilst, 2002; Darbyshire et al., 2013; see Fig. 7a). Aside from potentially distinct formation ages between the crust and its underlying mantle (Canil, 2008), the lack of correlation largely reflects the impact of secular evolution, such as growth and destruction, of the lithosphere (Griffin et al., 2009; Lee et al., 2011). Measurement techniques may also play a role: for example, the depth values obtained from body wave tomography are 60 km larger than those inferred from surface waves on average. This systematic shift, which is primarily due to the limited vertical

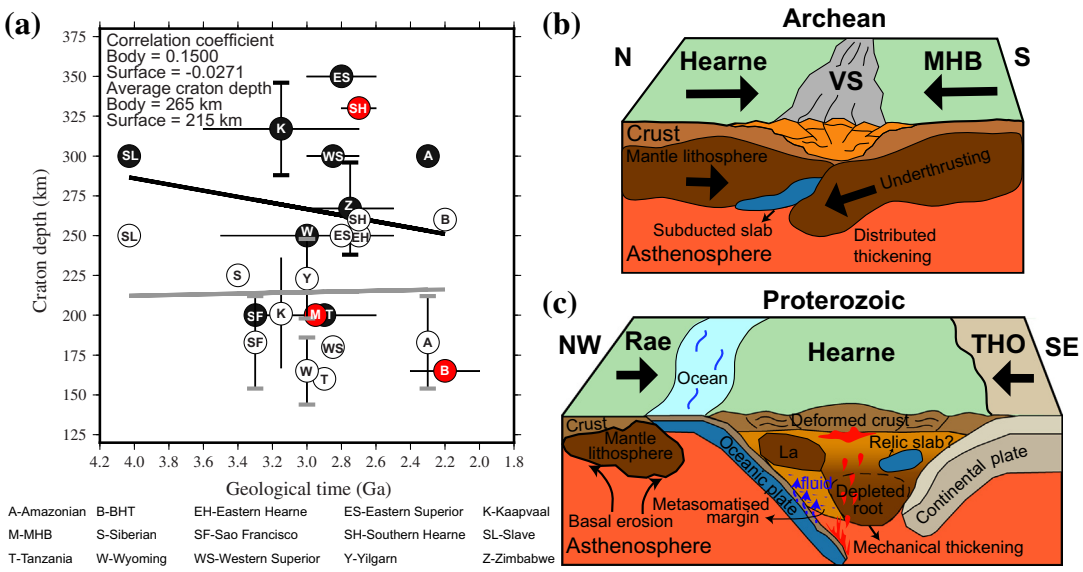

Fig. 7. (a) A summary of the depths and crustal ages of cratons. The craton depths are obtained from recent literature based on surface (white circle) and body (black circle) wave tomographic inversions (see Supporting information Text S2 for a complete reference list). The depth estimates from our study are marked by the red circles. The black and grey lines show the linear regressions for the body and surface waves, respectively. (b) A schematic diagram showing Archean lithospheric growth (subduction, collision and distributed thickening) of the Hearne province. (c) A model showing the Proterozoic lithospheric growth beneath the Hearne province, which involves mechanical thickening and modification of the upper mantle during the Proterozoic dual-subduction process. Lithosphere beneath the Rae craton (BHT) was eroded by the convective mantle flow. (For interpretation of the references to colour in this figure legend, the reader is referred to the web version of this article.)

resolution of body waves (McKenzie and Priestley, 2008), may be partially responsible for a deeper Hearne craton from this study (body wave; 330 km) relative to that from Bao and Eaton (2015; surface wave; 260 km). Regardless of the data types (body or surface waves), the southern Hearne province consistently ranks among the deepest cratons in the world (see Fig. 7a; Ritsema et al., 1998; Feng et al., 2004; Fishwick et al., 2005; Li and Burke, 2006; Priestley et al., 2006; Frederiksen et al., 2013; de Azevedo et al., 2015; Youssof et al., 2015). The thickness of its mantle lithosphere is, at a minimum, 100 km greater than those beneath the neighboring BHT and MHB. This substantial thickness variation within a relatively short (<150 km) lateral distance causes a major lithospheric depth gradient on either side of the Archean Hearne province along the NW-SE orientation (see Figs. 4c and 7a).

4.2. Assessments of earlier models of tectonic assembly

A deep Hearne craton, in conjunction with the low average velocities (−0.5–0.5%) in the crust and shallow mantle (see shaded area in Fig. 6b), is consistent with the regional tectonic framework involving reported tectonic assembly events during: 1) the Archean plate convergence between the MHB (3.8–2.6 Ga) and the Hearne province (2.71–1.78 Ga; Lemieux et al., 2000; Clowes et al., 2002; Gorman et al., 2002), and 2) the post-Archean (Proterozoic) dual-subduction and reworking of the Hearne craton (Boerner et al., 2000; Ross et al., 2000; Ross, 2002). The former process (Archean collision; Ross et al., 1991; Eaton et al., 1999a) is consistent with our observation of reduced seismic velocities overlying the deepest root beneath the southern Hearne province and the Archean suture zone of the VS (see Figs. 4c and 6b). In the same region, Gorman et al. (2002) reported a north dipping seismic reflector in the upper mantle and interpreted it as a relic subducted oceanic lithosphere. It is plausible that the fertile peridotite within the subducted slab or metasomatic fluids from slab dehydration could have enriched the overlying mantle (Fig. 7b), thereby lowering seismic velocity of an otherwise chemically-depleted (i.e., fast) craton (Jordan, 1979; Griffin et al., 2009). The resultant fertilized upper mantle is compatible with the increased mantle conductivity in this region (Nieuwenhuis et al., 2014). Following this subduction, the lithosphere near the collisional boundary (i.e., the VS) may have undergone distributed thickening (Pysklywec et al., 2002) in response to the continent-continent collision (see Fig. 7b).

Proterozoic (2.0–1.8 Ga) tectonic events (Fig. 7c) may have also impacted the growth of the lithospheric keel of the Hearne craton. It has been suggested that contemporaneous subduction took place along the STZ and THO during the terminal collisions that amalgamated the Hearne province with the Rae province to its NW (Ross et al., 1991; Eaton and Cassidy, 1996) and with the Superior province to its SE (Lucas et al., 1993; Corrigan et al., 2005; see Fig. 7c). The entrapment of Hearne between Rae and THO may have induced mechanical thickening (i.e., thickening in response to the horizontal shortening; Conrad, 2000) due to the compressive stresses exerted by the strong plate coupling (Ross, 2002; Bao and Eaton, 2015). During this process, the coeval tectonothermal events (Clowes et al., 2002; Ross, 2002) could significantly modify the mantle lithosphere, as suggested by the absence of Archean signature from mantle garnet xenocrysts (Canil et al., 2003) and increased mantle conductivity (Boerner et al., 2000), and further enhance the compositional differentiation of the Hearne craton (see Fig. 7c). For example, the margin of the Hearne craton (Lacombe domain) may have undergone metasomatic enrichment due to the transfer of fluids and melts from the underthrusting oceanic plate (i.e., the Thorsby domain; Ross, 2002; see Fig. 7c). A similar subduction-driven modification has been documented along the eastern margin of North American craton (Boyce et al., 2016).

The Precambrian tectonic history provides an ideal geological framework to interpret the observed velocity anomalies beneath the Hearne craton. More recent (Mesozoic) terrane accretion and subduction beneath the western margin of Laurentia could have significantly impacted the shallow mantle structure within the cratonic lithosphere. One such modification is documented in the Wyoming craton, which collided with the MHB during Archean assembly events along the GFTZ (see Fig. 1). It was suggested that the Wyoming lithosphere underwent delamination and the subsequent emplacement of an oceanic plateau in association with the subduction of Farallon slab (Humphreys et al., 2015). Considering the geographical affinity between the Wyoming craton and our study area, this process provides a simple and attractive explanation to most of the observed velocity anomalies. Under this assumption, the high velocity root of the Hearne province could

represent an accreted, basalt-depleted oceanic plate, while the overlying low velocities can be attributed to metasomatic enrichment induced by the fluid dehydration of the slab. However, this hypothesis remains speculative, as 1 there is limited geophysical evidence for the basement reactivation of the Hearne craton since the Paleoproterozoic (1.8 Ga; Ross and Eaton, 1999 and 2) the expected effect of the Farallon subduction would be the most significant along the southwest-northeast orientation rather than trench parallel (see cross-section BB' in Fig. 4). A further study involving more detailed geophysical imaging, geochronological dating and geodynamical modeling will be required to ascertain the effects of the Mesozoic subduction on the structure beneath the Precambrian cratons.

4.3. Lithospheric destruction in western Laurentia

In addition to the lithospheric growth events illustrated in Fig. 7b and c, the first-order difference in lithospheric thickness between the Hearne craton (~330 km) and its adjacent Precambrian domains (<200 km) may have been further enhanced by the subsequent destruction processes, most notably connective erosion (Artemieva and Mooney, 2002; Lee et al., 2011). Our observations fall within the bimodal distribution of craton thickness globally, which is interpreted as the bi-product of the preferential erosion of cratons with different sizes following the break-up of a supercontinent (Artemieva and Mooney, 2002). This hypothesis provides a partial explanation for a shallow lithosphere beneath the BHT, as a smaller BHT is subjected to greater erosion by the convective mantle flow than a larger Hearne province in response to possible asthenospheric upwelling and incipient rifting along the STZ (Flowers et al., 2006). This convective removal process may have been further enhanced by the metasomatic refertilization via the movements of melts or fluids (Foley, 2008; Lee et al., 2011), which would effectively reduce the bulk velocities of the lithospheric mantle in the vicinity of the BHT (e.g., beneath the WTR; see Fig. 4c for location). Melt generation was evidenced by the asthenospheric-derived silicate magma (Aulbach et al., 2004) and the subsequent Paleoproterozoic melt intrusion into the shallow lithosphere beneath the BHT (Welford and Clowes, 2006). This mechanism was invoked to explain the partial removal of the lithosphere beneath the central Rae craton (Liu et al., 2016).

5. Conclusion

A multi-scale finite-frequency tomography method, in combination with data from regional seismic arrays, enables us to conduct a high-resolution survey of the upper mantle beneath the southern WCSB. Our high-resolution P velocity model reveals distinct high velocities in connection with the lithosphere beneath the MHB, Hearne province and BHT. The lithospheric root beneath the Hearne craton extends down to a minimum depth of 300 km, whereas the lithosphere beneath the MHB and BHT are only about 180 km thick, resulting in sharp contrasts in lithospheric thickness surrounding the Hearne province. The deep high velocity root and substantially reduced crustal-shallow mantle velocities beneath the Hearne craton are consistent with earlier models of the tectonic assembly that involve episodes of subduction and continent-continent collision in the Precambrian. Lithospheric destruction processes (e.g., convective erosion) may have further enhanced the lithospheric thickness differences between the Hearne craton and its adjacent domains.

Funding

This study is supported by the Helmholtz-Alberta Initiative (HAI grant RES0019262).

Acknowledgments and data

The seismic data from USArray, RAVEN and CNSN networks are provided by IRIS Data Management Center and Canadian National Data Center. The travel-time data from CRANE and the tomographic model are available upon request to seismology group of the University of Alberta. We thank Thomas Chacko for helpful discussions. We thank Jacek Majorowicz for kindly sending us the regional heat flow data. We thank Andrew Frederiksen for constructive comments that improved the manuscript.

Appendix A. Supplementary data

Supplementary data to this article can be found online at http://dx.doi.org/10.1016/j.tecto.2017.01.006.

References

Arndt, N.T., Coltice, N., Helmstaedt, H., Gregoire, M., 2009. Origin of Archean subcontinental lithospheric mantle: some petrological constraints. Lithos 109 (1), 61–71.
Artemieva, I.M., Mooney, W.D., 2002. On the relations between cratonic lithosphere thickness, plate motions, and basal drag. Tectonophysics 358 (1), 211–231.
Aulbach, S., Griffin, W.L., O'Reilly, S.Y., McCandless, T.E., 2004. Genesis and evolution of the lithospheric mantle beneath the buffalo head terrane, Alberta (Canada). Lithos 77 (1), 413–451.
Bao, X., Eaton, D.W., 2015. Large variations in lithospheric thickness of western Laurentia: tectonic inheritance or collisional reworking? Precambrian Res. 266, 579–586.
Berman, R.G., Davis, W.J., Pehrsson, S., 2007. Collisional snowbird tectonic zone resurrected: growth of Laurentia during the 1.9 Ga accretionary phase of the Hudsonian orogeny. Geology 35 (10), 911–914.
Boerner, D.E., Craven, J.A., Kurtz, R.D., Ross, G.M., Jones, F.W., 1998. The great falls tectonic zone: suture or intracontinental shear zone? Can. J. Earth Sci. 35 (2), 175–183.
Boerner, D.E., Kurtz, R.D., Craven, J.A., Ross, G.M., Jones, F.W., Davis, W.J., 1999. Electrical conductivity in the Precambrian lithosphere of Western Canada. Science 283 (5402), 668–670.
Boerner, D.E., Kurtz, R.D., Craven, J.A., Ross, G.M., Jones, F.W., 2000. A synthesis of electromagnetic studies in the Lithoprobe Alberta Basement Transect: constraints on Paleoproterozoic indentation tectonics. Can. J. Earth Sci. 37 (11), 1509–1534.
Bostock, M.G., 1998. Mantle stratigraphy and evolution of the Slave province. J. Geophys. Res. Solid Earth 103 (B9), 21183–21200.
Bouzidi, Y., Schmitt, D.R., Burwash, R.A., Kanasewich, E.R., 2002. Depth migration of deep seismic reflection profiles: crustal thickness variations in Alberta. Can. J. Earth Sci. 39 (3), 331–350.
Boyce, A., Bastow, I.D., Darbyshire, F.A., Ellwood, A.G., Gilligan, A., Levin, V., Menke, W., 2016. Subduction beneath Laurentia modified the eastern North American cratonic edge: evidence from P wave and S wave tomography. J. Geophys. Res. Solid Earth 121, 5013–5030.
Boyd, F.R., 1989. Compositional distinction between oceanic and cratonic lithosphere. Earth Planet. Sci. Lett. 96 (1), 15–26.
Buhlmann, A.L., Cavell, P., Burwash, R.A., Creaser, R.A., Luth, R.W., 2000. Minette bodies and cognate mica-clinopyroxenite xenoliths from the Milk River area, southern Alberta: records of a complex history of the northernmost part of the Archean Wyoming craton. Can. J. Earth Sci. 37 (11), 1629–1650.
Canil, D., 2004. Mildly incompatible elements in peridotites and the origins of mantle lithosphere. Lithos 77 (1), 375–393.
Canil, D., 2008. Canada's craton: a bottoms-up view. GSA Today 18 (6), 4.
Canil, D., Schulze, D.J., Hall, D., Hearn Jr., B.C., Milliken, S.M., 2003. Lithospheric roots beneath western Laurentia: the geochemical signal in mantle garnets. Can. J. Earth Sci. 40 (8), 1027–1051.
Carlson, R.W., Irving, A.J., Schulze, D.J., Hearn, B.C., 2004. Timing of Precambrian melt depletion and Phanerozoic refertilization events in the lithospheric mantle of the Wyoming Craton and adjacent Central Plains Orogen. Lithos 77 (1), 453–472.
Carlson, R.W., Pearson, D.G., James, D.E., 2005. Physical, chemical, and chronological characteristics of continental mantle. Rev. Geophys. 43 (1).
Chen, Y., Gu, Y.J., Dokht, R.M.H., Sacchi, M.D., 2015. Crustal imprints of Precambrian orogenesis in western Laurentia. J. Geophys. Res. Solid Earth 120 (10), 6993–7012.
Chiao, L.-Y., Kuo, B.-Y., 2001. Multiscale seismic tomography. Geophys. J. Int. 145 (2), 517–527.
Clowes, R.M., Zelt, C.A., Amor, J.R., Ellis, R.M., 1995. Lithospheric structure in the southern Canadian Cordillera from a network of seismic refraction lines. Can. J. Earth Sci. 32 (10), 1485–1513.
Clowes, R.M., Burianyk, M.J., Gorman, A.R., Kanasewich, E.R., 2002. Crustal velocity structure from SAREX, the southern Alberta refraction experiment. Can. J. Earth Sci. 39 (3), 351–373.
Conrad, C.P., 2000. Convective instability of thickening mantle lithosphere. Geophys. J. Int. 143 (1), 52–70.
Cooper, C.M., Lenardic, A., Levander, A., Moresi, L., 2006. Creation and preservation of cratonic lithosphere: seismic constraints and geodynamic models. Archean Geodynamics and Environments, pp. 75–88.
Corrigan, D., Hajnal, Z., Németh, B., Lucas, S.B., 2005. Tectonic framework of a Paleoproterozoic arc-continent to continent-continent collisional zone, Trans-

Hudson Orogen, from geological and seismic reflection studies. Can. J. Earth Sci. 42 (4), 421–434.
Corrigan, D., Pehrsson, S., Wodicka, N., De Kemp, E., 2009. The Palaeoproterozoic Trans-Hudson Orogen: a prototype of modern accretionary processes. Geol. Soc. Lond., Spec. Publ. 327 (1), 457–479.
Dahlen, F.A., Hung, S.-H., Nolet, G., 2000. Fréchet kernels for finite-frequency traveltimes—I. Theory. Geophys. J. Int. 141 (1).
Dalton, C.A., Gaherty, J.B., Courtier, A.M., 2011. Crustal VS structure in northwestern Canada: imaging the Cordillera-craton transition with ambient noise tomography. J. Geophys. Res. Solid Earth 116 (B12).
Darbyshire, F.A., Eaton, D.W., Bastow, I.D., 2013. Seismic imaging of the lithosphere beneath Hudson Bay: episodic growth of the Laurentian mantle keel. Earth Planet. Sci. Lett. 373, 179–193.
Davis, W.J., Jones, A.G., Bleeker, W., Grütter, H., 2003. Lithosphere development in the Slave craton: a linked crustal and mantle perspective. Lithos 71 (2), 575–589.
de Azevedo, P.A., Rocha, M.P., Soares, J.E.P., Fuck, R.A., 2015. Thin lithosphere between the Amazonian and São Francisco cratons, in central Brazil, revealed by seismic P-wave tomography. Geophys. J. Int. 201 (1), 61–69.
Dickinson, W.R., 2004. Evolution of the North American cordillera. Annu. Rev. Earth Planet. Sci. 32, 13–45.
Eaton, D.W., Cassidy, J.F., 1996. A relic Proterozoic subduction zone in western Canada: new evidence from seismic reflection and receiver function data. Geophys. Res. Lett. 23 (25), 3791–3794.
Eaton, D.W., Ross, G.M., Clowes, R.M., 1999a. Seismic-reflection and potential-field studies of the Vulcan structure, western Canada: a Paleoproterozoic Pyrenees? J. Geophys. Res. Solid Earth 104 (B10), 23255–23269.
Eaton, D.W., Ross, G.M., Hope, J., 1999b. The rise and fall of a cratonic arch: a regional seismic perspective on the Peace River Arch, Alberta. Bull. Can. Petrol. Geol. 47 (4), 346–361.
Eaton, D.W., Ross, G.M., Cook, F.A., VanderVelden, A., 2000. Seismic imaging of the upper mantle beneath the Rocky Mountain foreland, southwestern Alberta. Can. J. Earth Sci. 37 (11), 1493–1507.
Feng, M., Assumpçao, M., Van der Lee, S., 2004. Group-velocity tomography and lithospheric S-velocity structure of the South American continent. Phys. Earth Planet. Inter. 147 (4), 315–331.
Fischer, K.M., Ford, H.A., Abt, D.L., Rychert, C.A., 2010. The lithosphere-asthenosphere boundary. Annu. Rev. Earth Planet. Sci. 38, 551–575.
Fishwick, S., Kennett, B.L.N., Reading, A.M., 2005. Contrasts in lithospheric structure within the Australian craton—insights from surface wave tomography. Earth Planet. Sci. Lett. 231 (3), 163–176.
Flowers, R.M., Bowring, S.A., Williams, M.L., 2006. Timescales and significance of high-pressure, high-temperature metamorphism and mafic dike anatexis, Snowbird tectonic zone, Canada. Contrib. Mineral. Petrol. 151 (5), 558–581.
Foley, S.F., 2008. Rejuvenation and erosion of the cratonic lithosphere. Nat. Geosci. 1 (8), 503–510.
Foster, D.A., Mueller, P.A., Mogk, D.W., Wooden, J.L., Vogl, J.J., 2006. Proterozoic evolution of the western margin of the Wyoming craton: implications for the tectonic and magmatic evolution of the northern Rocky Mountains. Can. J. Earth Sci. 43 (10), 1601–1619.
Frederiksen, A., Bostock, M., Cassidy, J., 2001. S-wave velocity structure of the Canadian upper mantle. Phys. Earth Planet. Inter. 124 (3), 175–191.
Frederiksen, A.W., Bollmann, T., Darbyshire, F., Lee, S., 2013. Modification of continental lithosphere by tectonic processes: a tomographic image of central North America. J. Geophys. Res. Solid Earth 118 (3), 1051–1066.
Gao, S., Rudnick, R.L., Carlson, R.W., McDonough, W.F., Liu, Y.-S., 2002. Re–Os evidence for replacement of ancient mantle lithosphere beneath the North China craton. Earth Planet. Sci. Lett. 198 (3), 307–322.
Gerya, T., 2014. Precambrian geodynamics: concepts and models. Gondwana Res. 25 (2), 442–463.
Gorman, A.R., Clowes, R.M., Ellis, R.M., Henstock, T.J., Spence, G.D., Keller, G.R., Levander, A., Snelson, C.M., Burianyk, M.J.A., Kanasewich, E.R., 2002. Deep probe: imaging the roots of western North America. Can. J. Earth Sci. 39 (3), 375–398.
Gray, R., Pysklywec, R.N., 2010. Geodynamic models of Archean continental collision and the formation of mantle lithosphere keels. Geophys. Res. Lett. 37 (19).
Griffin, W.L., O'Reilly, S.Y., Abe, N., Aulbach, S., Davies, R.M., Pearson, N.J., Doyle, B.J., Kivi, K., 2003. The origin and evolution of Archean lithospheric mantle. Precambrian Res. 127 (1), 19–41.
Griffin, W.L., O'reilly, S.Y., Afonso, J.C., Begg, G.C., 2009. The composition and evolution of lithospheric mantle: a re-evaluation and its tectonic implications. J. Petrol. 50 (7), 1185–1204.
Gu, Y.J., Shen, L., 2015. Noise correlation tomography of Southwest Western Canada Sedimentary Basin. Geophys. J. Int. 202 (1), 142–162.
Gu, Y.J., Okeler, A., Shen, L., Contenti, S., 2011. The Canadian Rockies and Alberta network (CRANE): new constraints on the Rockies and western Canada sedimentary basin. Seismol. Res. Lett. 82 (4), 575–588.
Gu, Y.J., Zhang, Y., Sacchi, M.D., Chen, Y., Contenti, S., 2015. Sharp mantle transition from cratons to Cordillera in southwestern Canada. J. Geophys. Res. Solid Earth 120 (7), 5051–5069.
Hammer, P.T.C., Clowes, R.M., Cook, F.A., Vasudevan, K., van der Velden, A.J., 2011. The big picture: a lithospheric cross section of the North American continent. GSA Today 21 (6), 4–10.
Hanmer, S., Williams, M., Kopf, C., 1995. Striding-Athabasca mylonite zone: implications for the Archean and Early Proterozoic tectonics of the western Canadian Shield. Can. J. Earth Sci. 32 (2), 178–196.
Helmstaedt, H., Schulze, D.J., 1989. Southern African kimberlites and their mantle sample: implications for Archean tectonics and lithosphere evolution. Kimberlites and Related Rocks. Vol. 1, pp. 358–368.
Hoffman, P.F., 1988. United plates of America, the birth of a craton-Early Proterozoic assembly and growth of Laurentia. Annu. Rev. Earth Planet. Sci. 16, 543–603.
Hoffman, P.F., 1989. Precambrian geology and tectonic history of North America. Geol. North Am. 447–512.
Hoffman, P.F., 1990. Geological constraints on the origin of the mantle root beneath the Canadian Shield. Philos. Trans. R. Soc. Lond. A 331 (1620), 523–532.
Hope, J., Eaton, D., 2002. Crustal structure beneath the Western Canada Sedimentary Basin: constraints from gravity and magnetic modelling. Can. J. Earth Sci. 39 (3), 291–312.
Hopper, E., Fischer, K.M., 2015. The meaning of midlithospheric discontinuities: a case study in the northern US craton. Geochem. Geophys. Geosyst. 16 (12), 4057–4083.
Humphreys, E.D., Schmandt, B., Bezada, M.J., Perry-Houts, J., 2015. Recent craton growth by slab stacking beneath Wyoming. Earth Planet. Sci. Lett. 429, 170–180.
Hung, S.H., Dahlen, F., Nolet, G., 2000. Frechet kernels for finite-frequency traveltimesII. Examples. Geophys. J. Int. 141 (1), 175–203.
Hung, S.H., Shen, Y., Chiao, L.-Y., 2004. Imaging seismic velocity structure beneath the Iceland hot spot: a finite frequency approach. J. Geophys. Res. Solid Earth 109 (B8).
Hung, S.H., Chen, W.-P., Chiao, L.-Y., Tseng, T.-L., 2010. First multi-scale, finite-frequency tomography illuminates 3-D anatomy of the Tibetan Plateau. Geophys. Res. Lett. 37 (6).
Hung, S.H., Chen, W.-P., Chiao, L.-Y., 2011. A data-adaptive, multiscale approach of finite-frequency, traveltime tomography with special reference to P and S wave data from central Tibet. J. Geophys. Res. Solid Earth 116 (B6).
Hyndman, R., 2010. The consequences of Canadian Cordillera thermal regime in recent tectonics and elevation: a review. Can. J. Earth Sci. 47 (5), 621–632.
Hyndman, R.D., Currie, C.A., 2011. Why is the North America Cordillera high? Hot backarcs, thermal isostasy, and mountain belts. Geology 39 (8), 783–786.
Jordan, T.H., 1975. The continental tectosphere. Rev. Geophys. 13 (3), 1–12.
Jordan, T.H., 1978. Composition and development of the continental tectosphere. Nature 274 (5671), 544–548.
Jordan, T.H., 1979. Mineralogies, densities and seismic velocities of garnet lherzolites and their geophysical implications: The Mantle Sample. Inclusion in Kimberlites and Other Volcanics, pp. 1–14.
Jordan, T.H., 1988. Structure and formation of the continental tectosphere. J. Petrol. (1), 11–37.
Kanasewich, E.R., Clowes, R.M., McCloughan, C.H., 1969. A buried Precambrian rift in western Canada. Tectonophysics 8 (4), 513–527.
Kao, H., Behr, Y., Currie, C.A., Hyndman, R., Townend, J., Lin, F.C., Ritzwoller, M.H., Shan, S.J., He, J., 2013. Ambient seismic noise tomography of Canada and adjacent regions: part I. Crustal structures. J. Geophys. Res. Solid Earth 118 (11), 5865–5887.
Kennett, B., Engdahl, E., Buland, R., 1995. Constraints on seismic velocities in the Earth from traveltimes. Geophys. J. Int. 122 (1), 108–124.
King, S.D., 2005. Archean cratons and mantle dynamics. Earth Planet. Sci. Lett. 234 (1), 1–14.
Lee, C.-T.A., Luffi, P., Chin, E.J., 2011. Building and destroying continental mantle. Annu. Rev. Earth Planet. Sci. 39, 59–90.
Lemieux, S., Ross, G.M., Cook, F.A., 2000. Crustal geometry and tectonic evolution of the Archean crystalline basement beneath the southern Alberta Plains, from new seismic reflection and potential-field studies. Can. J. Earth Sci. 37 (11), 1473–1491.
Lewis, T.J., Hyndman, R.D., Flück, P., 2003. Heat flow, heat generation, and crustal temperatures in the northern Canadian Cordillera: thermal control of tectonics. J. Geophys. Res. Solid Earth 108 (B6).
Lewry, J.F., Hajnal, Z., Green, A., Lucas, S.B., White, D., Stauffer, M.R., Ashton, K.E., Weber, W., Clowes, R., 1994. Structure of a Paleoproterozoic continent-continent collision zone: a LITHOPROBE seismic reflection profile across the Trans-Hudson Orogen, Canada. Tectonophysics 232 (1–4), 143–160.
Li, A., Burke, K., 2006. Upper mantle structure of southern Africa from Rayleigh wave tomography. J. Geophys. Res. Solid Earth 111 (B10).
Liu, Q., Gu, Y.J., 2012. Seismic imaging: from classical to adjoint tomography. Tectonophysics 566, 31–66.
Liu, J., Riches, A.J.V., Pearson, D.G., Luo, Y., Kienlen, B., Kjarsgaard, B.A., Stachel, T., Armstrong, J.P., 2016. Age and evolution of the deep continental root beneath the central Rae craton, northern Canada. Precambrian Res. 272, 168–184.
Lucas, S.B., Green, A., Hajnal, Z., White, D., Lewry, J., Ashton, K., Weber, W., Clowes, R., 1993. Deep seismic profile across a Proterozoic collision zone: surprises at depth. Nature 363 (6427), 339–342.
Majorowicz, J.A., 2016. Heat flow–heat production relationship not found: what drives heat flow variability of the Western Canadian foreland basin? Int. J. Earth Sci. 1–14.
Majorowicz, J., Chan, J., Crowell, J., Gosnold, W., Heaman, L.M., Kück, J., Nieuwenhuis, G., Schmitt, D.R., Unsworth, M., Walsh, N., 2014. The first deep heat flow determination in crystalline basement rocks beneath the Western Canadian Sedimentary Basin. Geophys. J. Int. 197 (2), 731–747.
McKenzie, D., Priestley, K., 2008. The influence of lithospheric thickness variations on continental evolution. Lithos 102 (1), 1–11.
Meqbel, N.M., Egbert, G.D., Wannamaker, P.E., Kelbert, A., Schultz, A., 2014. Deep electrical resistivity structure of the northwestern US derived from 3-D inversion of USArray magnetotelluric data. Earth Planet. Sci. Lett. 402, 290–304.
Mercier, J.-P., Bostock, M., Cassidy, J., Dueker, K., Gaherty, J., Garnero, E., Revenaugh, J., Zandt, G., 2009. Body-wave tomography of western Canada. Tectonophysics 475 (3), 480–492.
Montelli, R., Nolet, G., Dahlen, F.A., Masters, G., Engdahl, E.R., Hung, S.-H., 2004. Finite-frequency tomography reveals a variety of plumes in the mantle. Science 303 (5656), 338–343.
Mueller, P.A., Frost, C.D., 2006. The Wyoming Province: a distinctive Archean craton in Laurentian North America. Can. J. Earth Sci. 43 (10), 1391–1397.

Mueller, P.A., Heatherington, A.L., Kelly, D.M., Wooden, J.L., Mogk, D.W., 2002. Paleoproterozoic crust within the great falls tectonic zone: implications for the assembly of southern Laurentia. Geology 30 (2), 127–130.
Nieuwenhuis, G., Unsworth, M.J., Pana, D., Craven, J., Bertrand, E., 2014. Three-dimensional resistivity structure of Southern Alberta, Canada: implications for Precambrian tectonics. Geophys. J. Int. 197 (2), 838–859.
Paige, C.C., Saunders, M.A., 1982. LSQR: an algorithm for sparse linear equations and sparse least squares. ACM Trans. Math. Softw. 8 (1), 43–71.
Pearson, D.G., Wittig, N., 2008. Formation of Archaean continental lithosphere and its diamonds: the root of the problem. J. Geol. Soc. 165 (5), 895–914.
Pollack, H.N., 1986. Cratonization and thermal evolution of the mantle. Earth Planet. Sci. Lett. 80 (1–2), 175–182.
Priestley, K., Debayle, E., 2003. Seismic evidence for a moderately thick lithosphere beneath the Siberian platform. Geophys. Res. Lett. 30 (3).
Priestley, K., McKenzie, D., Debayle, E., 2006. The state of the upper mantle beneath southern Africa. Tectonophysics 416 (1), 101–112.
Pysklywec, R.N., Beaumont, C., Fullsack, P., 2002. Lithospheric deformation during the early stages of continental collision: numerical experiments and comparison with South Island, New Zealand. J. Geophys. Res. Solid Earth 107 (B7) (p. ETG 3-1-ETG 3-19).
Ritsema, J., Nyblade, A.A., Owens, T.J., Langston, C.A., VanDecar, J.C., 1998. Upper mantle seismic velocity structure beneath Tanzania, East Africa: implications for the stability of cratonic lithosphere. J. Geophys. Res. Solid Earth 103 (B9), 21201–21213.
Ross, G.M., 2002. Evolution of Precambrian continental lithosphere in Western Canada: results from Lithoprobe studies in Alberta and beyond. Can. J. Earth Sci. 39 (3), 413–437.
Ross, G.M., Eaton, D.W., 1997. Winagami reflection sequence: seismic evidence for postcollisional magmatism in the Proterozoic of western Canada. Geology 25 (3), 199–202.
Ross, G.M., Eaton, D.W., 1999. Basement reactivation in the Alberta Basin: observational constraints and mechanical rationale. Bull. Can. Petrol. Geol. 47 (4), 391–411.
Ross, G.M., Parrish, R.R., Villeneuve, M.E., Bowring, S.A., 1991. Geophysics and geochronology of the crystalline basement of the Alberta Basin, western Canada. Can. J. Earth Sci. 28 (4), 512–522.
Ross, G.M., Milkereit, B., Eaton, D., White, D., Kanasewich, E.R., Burianyk, M.J.A., 1995. Paleoproterozoic collisional orogen beneath the western Canada sedimentary basin imaged by Lithoprobe crustal seismic-reflection data. Geology 23 (3), 195–199.
Ross, G.M., Eaton, D.W., Boerner, D.E., Miles, W., 2000. Tectonic entrapment and its role in the evolution of continental lithosphere: an example from the Precambrian of western Canada. Tectonics 19 (1), 116–134.
Sambridge, M., Drijkoningen, G., 1992. Genetic algorithms in seismic waveform inversion. Geophys. J. Int. 109 (2), 323–342.
Schultz, R., Stern, V., 2015a. The Regional Alberta Observatory for Earthquake Studies Network (RAVEN). CSEG Recorder. Vol. 40(8), pp. 34–37.
Schultz, R., Stern, V., Gu, Y.J., 2014. An investigation of seismicity clustered near the Cordel field, west central Alberta, and its relation to a nearby disposal well. J. Geophys. Res. Solid Earth 119 (4), 3410–3423.
Schultz, R., Stern, V., Gu, Y.J., Eaton, D., 2015b. Detection threshold and location resolution of the Alberta geological survey earthquake catalogue. Seismol. Res. Lett. 86 (2A), 385–397.
Shragge, J., Bostock, M., Bank, C., Ellis, R., 2002. Integrated teleseismic studies of the southern Alberta upper mantle. Can. J. Earth Sci. 39 (3), 399–411.
Simons, F.J., Van Der Hilst, R.D., 2002. Age-dependent seismic thickness and mechanical strength of the Australian lithosphere. Geophys. Res. Lett. 29 (11).
Sleep, N.H., 2005. Evolution of the continental lithosphere. Annu. Rev. Earth Planet. Sci. 33, 369–393.
Snyder, D.B., Craven, J.A., Pilkington, M., Hillier, M.J., 2015. The 3-dimensional construction of the Rae craton, central Canada. Geochem. Geophys. Geosyst. 16 (10), 3555–3574.
Tesoniero, A., Auer, L., Boschi, L., Cammarano, F., 2015. Hydration of marginal basins and compositional variations within the continental lithospheric mantle inferred from a new global model of shear and compressional velocity. J. Geophys. Res. Solid Earth 120 (11), 7789–7813.
Türkoglu, E., Unsworth, M., Pana, D., 2009. Deep electrical structure of northern Alberta (Canada): implications for diamond exploration. Can. J. Earth Sci. 46 (2), 139–154.
VanDecar, J.C., Crosson, R.S., 1990. Determination of teleseismic relative phase arrival times using multi-channel cross-correlation and least squares. Bull. Seismol. Soc. Am. 80 (1), 150–169.
Villeneuve, M.E., Ross, G.M., Parrish, R.R., Theriault, R.J., Miles, W., Broome, J., 1993. Geophysical subdivision, U–Pb geochronology and Sm–Nd isotope geochemistry of the crystalline basement of the Western Canada Sedimentary Basin, Alberta and northeastern British Columbia. Geol. Surv. Can. Bull. 447, 86.
Wang, R., Gu, Y.J., Schultz, R., Kim, A., Atkinson, G., 2016. Source analysis of a potential hydraulic-fracturing-induced earthquake near Fox Creek, Alberta. Geophys. Res. Lett.
Welford, J.K., Clowes, R.M., 2006. Three-dimensional seismic reflection investigation of the upper crustal Winagami sill complex of northwestern Alberta, Canada. Geophys. J. Int. 166 (1), 155–169.
Whitmeyer, S.J., Karlstrom, K.E., 2007. Tectonic model for the Proterozoic growth of North America. Geosphere 3 (4), 220–259.
Wright, G.N., McMechan, M.E., Potter, D.E.G., 1994. Structure and architecture of the Western Canada sedimentary basin. Geological Atlas of the Western Canada Sedimentary Basin. vol. 4, pp. 25–40.
Youssof, M., Thybo, H., Artemieva, I.M., Levander, A., 2015. Upper mantle structure beneath southern African cratons from seismic finite-frequency P-and S-body wave tomography. Earth Planet. Sci. Lett. 420, 174–186.
Yuan, H., Romanowicz, B., 2010. Lithospheric layering in the North American craton. Nature 466 (7310), 1063–1068.
Zhou, Y., Dahlen, F.A., Nolet, G., Laske, G., 2005. Finite-frequency effects in global surface-wave tomography. Geophys. J. Int. 163 (3), 1087–1111.